Implication of Sphingomyelin/Ceramide Molar Ratio on the Biological Activity of Sphingomyelinase

Beate Boulgaropoulos, Heinz Amenitsch, Peter Laggner, and Georg Pabst*
Institute of Biophysics and Nanosystems Research, Austrian Academy of Sciences, Graz, Austria

ABSTRACT Sphingolipid signaling plays an important, yet not fully understood, role in diverse aspects of cellular life. Sphingomyelinase is a major enzyme in these signaling pathways, catalyzing hydrolysis of sphingomyelin to ceramide and phosphocholine. To address the related membrane dynamical structural changes and their feedback to enzyme activity, we have studied the effect of enzymatically generated ceramide in situ on the properties of a well-defined lipid model system. We found a gel-phase formation that was about four times faster than ceramide generation due to ceramide-sphingomyelin pairing. The gel-phase formation slowed down when the ceramide molar ratios exceeded those of sphingomyelin and stopped just at the solubility limit of ceramide, due to unfavorable pairwise interactions of ceramide with itself and with monounsaturated phosphatidylcholine. A remarkable correlation to in vitro experiments suggests a regulation of sphingomyelinase activity based on the sphingomyelin/ceramide molar ratio.

INTRODUCTION

Sphingolipids are ubiquitously present in all mammalian cells and play an important role in the regulation of diverse cellular functions (1–4). Sphingomyelin (SM) is a major lipid component of plasma membranes and is considered to be extensively located in membrane rafts, where it helps to assemble signaling complexes (5,6). Of particular interest is the enzymatic degradation of SM by sphingomyelinase (SMase) to ceramide (Cer) and phosphocholine and the consequences of this degradation for the lateral heterogeneity of membranes. Various cellular processes have been related to SMase activity, among which, most prominently, is apoptosis (programmed cell death) (1–3). Apoptosis follows a characteristic morphological pathway and can be triggered by diverse stimuli, like death-receptor clustering, hypoxia, DNA damage with chemotherapeutic agents, or γ–radiation (7). Apoptosis is characterized by several key phases. In the initiator phase, the cells maintain their morphology to a large extent. Rapid and transient Cer formation by SMase activity facilitates death-receptor clustering at the membrane surface, possibly by the Cer property of stabilizing membrane rafts (8,9). Most recently, we were able to show that Cer generation might also indirectly affect the activity of proteins not located in rafts (10). Further, Cer may act as a second messenger during this stage (2,3). In the effector phase, plasma membranes lose the asymmetric lipid distribution, and neutral SMase (nSMase) generates Cer in the inner leaflet at the plasma membrane. The Cer formation in this apoptotic phase occurs slowly and continuously (2). Cer levels increase significantly, leading to membrane blebbing and apoptotic body formation. Finally, the execution phase of apoptosis is distinguished by continuous blebbing and vesiculation paired with cholesterol efflux from the membrane (2). Another characteristic is shrinking of the nucleus, constriction of apoptotic bodies, and, finally, the disposal of the cell. Details of apoptosis, however, seem to depend strongly on the type of apoptotic stimulus, as well as on the cell type (11,12).

Previous biophysical studies on model membranes of well-defined lipid composition showed that enzymatic fragmentation of SM leads to vesicle aggregation (13) and blebbing (14), very similar to the cellular events observed during apoptosis. Most recently, complex morphological membrane changes, involving stable Cer-rich and metastable SM-rich domains, respectively, have been reported in ternary lipid mixtures of dioleoyl phosphatidylcholine, SM, and cholesterol (15). A direct coupling of the timeline of the chemical modifications at the molecular level to membrane domain formation is presently missing, however. Further, it is not entirely clear whether the various labeling techniques applied in previous studies on SMase activity influence the observed phase behavior (16–18).

To address these gaps in our understanding, we performed an in situ, label-free study of the SMase activity profile in mammalian model membranes composed of an equimolar mixture of palmitoyl oleoyl phosphatidylcholine (POPC) and egg-SM. Although cholesterol is a major component of mammalian membranes and, like SM, is supposed to be extensively located in membrane rafts (5,6), it was deliberately excluded from this study, because POPC/SM/cholesterol membranes in a certain cholesterol concentration range exhibit a macroscopic fluid-fluid phase separation (15) that complicates time-resolved diffraction data analysis, and because it is important to understand the system in the absence of cholesterol. Enzymatic hydrolysis of SM was induced by the well-characterized nSMase from *Bacillus cereus* (19). The chemical and structural changes were

Submitted March 2, 2010, and accepted for publication April 15, 2010.

*Correspondence: georg.pabst@oeaw.ac.at

Editor: Thomas J. McIntosh.

0006-3495/10/07/0499/8 $2.00

doi: 10.1016/j.bpj.2010.04.028

addressed by a combination of high-performance thin-layer chromatography (HPTLC) and time-resolved x-ray diffraction. We observed interdependent kinetics on different lengthscales, strongly correlated with the SM/Cer molar ratio. Up to molar ratios of SM/Cer = 1, we found a gel-phase formation that proceeds four times faster than SM hydrolysis by SMase. At higher Cer levels, no further changes of the gel-phase domain size were observed, and the membrane structural parameters slowly approached an equilibrium state. Hydrolysis of SM was stopped just before the solubility limit of Cer was exceeded. Qualitative and quantitative agreement of our findings with those of cell biological experiments suggests that the biological activity of SMase depends strictly on the evolving SM/Cer molar ratio.

METHODS

Materials and sample preparation

POPC, egg-SM, and C16:0 Cer (*N*-palmitoyl-d-*erythro*-sphingosine) were purchased from Avanti Polar Lipids (Birmingham, AL) and used without further purification. nSMase from *Bacillus cereus* was obtained from Sigma Aldrich (St. Louis, MO) as lyophilized powder. All other chemicals (salts, solvents in pro analysis quality) and polyethylene glycol (PEG, molecular mass 8000) were from Sigma Aldrich. Purified water (18 MΩ/cm; UHQ PS, USF Elga, Wycombe, UK) was used for all liposomal preparations.

Dry lipid films of two different sample types were prepared as described previously (10). The first sample type was a binary, equimolar mixture of POPC and SM for the enzymatic reaction. The second sample type was a dispersion of multilamellar vesicles (MLVs) with a known amount of C16:0 Cer in a POPC/SM mixture for reference measurements. The lipid films containing Cer were hydrated in 20 mM Na-phosphate buffer (130 mM NaCl, pH 7.4), and the films for enzyme reaction experiments in 10 mM HEPES buffer (200 mM NaCl, 2 mM $MgCl_2$, and 10 mM $CaCl_2$, pH 6.8), using standard procedures yielding a total lipid concentration of 50 mg/ml. The POPC/SM vesicles for the SMase reaction were transformed into large unilamellar vesicles (LUVs) by 29 extrusion cycles through a 100-nm membrane filter (Nucleopore, Whatman International, Maidstone, United Kingdom) (see Fig. S1 *A* in the Supporting Material). Their average size was 120 nm, with polydispersity index 0.135, as determined by photon correlation spectroscopy on a Zetasizer 3000 HAS (Malvern Instruments, Herrenberg, Germany). LUVs were subsequently concentrated to ~70 mg/ml by centrifugation through a prerinsed centricon centrifugal filter device with an Ultracel YM-30 membrane (Millipore, Carrigtwohill, Ireland) (nominal molecular weight limit 30,000, 4500 g, 20 min). Finally, 10 U of nSMase was dissolved in 70 μL of the same buffer used for the LUV preparation, but containing, in addition, 2 mM *o*-phenanthroline to inhibit traces of contaminant phospholipase C activity of the enzyme (20).

HPTLC

HPTLC was performed on a fully automated system from CAMAG (Muttenz, Switzerland). HPTLC plates (silica gel 60 F 254) were from Merck (Darmstadt, Germany), and samples were sprayed automatically with 150 nL/s. During the experiment, well-defined amounts of the aqueous reaction batch were transferred into organic stop-solution ($CHCl_3$/MeOH = 2/1) and rigorously vortex-mixed for at least 3 min. Plates were developed with $CHCl_3$/MeOH/H_2O/CH_3COOH (65/25/4/1 v/v/v/v). Postchromatographic derivatization was performed with $CuSO_4$ (10%) in H_3PO_4 (4%), followed by 10 min incubation at 190°C. Peaks were scanned with a wavelength of 450 nm and quantified by relating peak height and area of the unknown lipid bands to those of POPC, SM, and C16:0 Cer standards. The minimum and maximum lipid amounts detected on the plate were ~0.1 μg and 1 μg, respectively. SM hydrolysis and Cer formation were fitted to a hyperbolic growth $C(t) = C_0 + Pt/(\tau_H + t)$, where C_0 is the offset, P the saturation level of the enzymatic turnover, and τ_H the time where half of the fragmentation is achieved.

X-ray diffraction

Time-resolved small- and wide-angle x-ray scattering (SWAXS) experiments were performed at the Austrian SAXS beamline at Elettra (Trieste, Italy). Two linear detectors were used to cover the scattering vectors, q, from 0.01 Å^{-1} to 0.6 Å^{-1} and 0.67 Å^{-1} to 1.95 Å^{-1} for SAXS and WAXS, respectively. Alternatively, a mar300 (Marresearch, Norderstedt, Germany) image plate detector was used for static experiments. Procedures for angular calibration, sample holders, and primary data reduction were described previously (10). Samples containing SMase were prepared by mixing LUV and enzyme solutions. Reaction batches were rapidly transferred to the sample holder, and measurements were started ~70 s after mixing. Diffraction patterns of 10-s exposure time were taken every minute. The exposure time with the image plate detector was set to 60 s. These samples were equilibrated at 37°C for 10 min before measurement. No signatures of radiation damage were observed during or after any experiment.

Selected SAXS data were analyzed in terms of a full q-range model (21,22) by a superposition of positionally correlated and positionally uncorrelated bilayers

$$I(q) \propto \left[(1 - p_{\text{diff}}) \frac{S(q)|F(q)|^2}{q^2} + p_{\text{diff}} \frac{|F(q)|^2}{q^2} \right] \qquad (1)$$

$S(q)$ describes the structure factor due to the positional correlations and $F(q)$ the form factor due to the modulation of the electron density across the bilayers. A modified Callié theory structure factor and a simple Gaussian electron density profile model were applied, as detailed previously (21,22). p_{diff} is constrained to the interval (0, 1). For $0 < p_{\text{diff}} < 1$, diffuse scattering, originating from positionally uncorrelated bilayers due to defects in MLVs and/or unilamellar vesicles, is accounted for, as is MLV scattering. Hence, p_{diff} gives a lower limit for the fraction of unilamellar vesicles in the lipid dispersion.

High-frequency noise was removed from WAXS data as described previously (23). A constant background was defined by a linear fit in a narrow range of the WAXS gel peak and subsequently subtracted from the WAXS data. Peak parameters were derived from Lorentz fits. In a similar way, SAXS peaks were analyzed using Lorentzian functions. The full width at half-maximum of the peaks, Δq, was corrected for the instrumental resolution, $\delta q = 2.2 \times 10^{-3}$ Å^{-1}, and used to calculate the average domain size (correlation length) (24), $L = 2\pi/\sqrt{\Delta q^2 - \delta q^2}$. Finally, the average number of layers was estimated from the SAXS data, applying $N_{\text{layer}} = L_{\text{SAXS}}/d$, where d is the lamellar repeat distance. The average number of positionally correlated lipids/gel-phase domain was estimated from $N_{\text{lip}} = L_{\text{WAXS}}/\sqrt{A}$, and the lateral area/lipid was calculated from the WAXS peak position by $A = 16\pi^2/(\sqrt{3}q_{\text{WAXS}}^2)$ (25).

Static SAXS measurements were also performed on a laboratory-based SWAXS camera (System 3, Hecus X-ray Systems, Graz, Austria). Samples were equilibrated for 10 min before measurement. Exposure times were 3000 s.

RESULTS

All experiments were performed at 37°C. In the following, we present the experimental findings on different hierarchical levels.

Changes on the molecular level

Enzymatic hydrolysis of SM was started by adding 30 μL of the large unilamellar vesicle (LUV) dispersion to 70 μL

enzyme solution. This gave a reaction batch with a lipid concentration of 27.3 mM and an enzyme activity of 100 U/mL (7.3 U/μmol SM). Fig. 1 presents the reaction progress of SM fragmentation and C16:0 Cer production as determined by HPTLC. Within the first ~150 min, total Cer levels increased rapidly, nearly reaching the plateau value of 86 $\pm$ 5%, as determined by a hyperbolic fit to the SM fragmentation data. The corresponding time constant was $\tau_H = 12$ min, i.e., ~43% of the original SM lipids were hydrolyzed after 12 min. C16:0 Cer levels increased with a similar time constant and saturated at 65 $\pm$ 8%. This value agrees well with the amount of SM fragmentation, as the fraction of C16:0 acyl chains of egg-SM is 84%, according to data from the supplier. It is interesting to compare these findings to SM degradation measurements of a biological system undergoing apoptosis. We found a remarkable agreement with published results on human leukemia cells (26), both in terms of kinetics and final SM levels (Fig. 1). Very similar results were also reported in fibroblast cells (27,28).

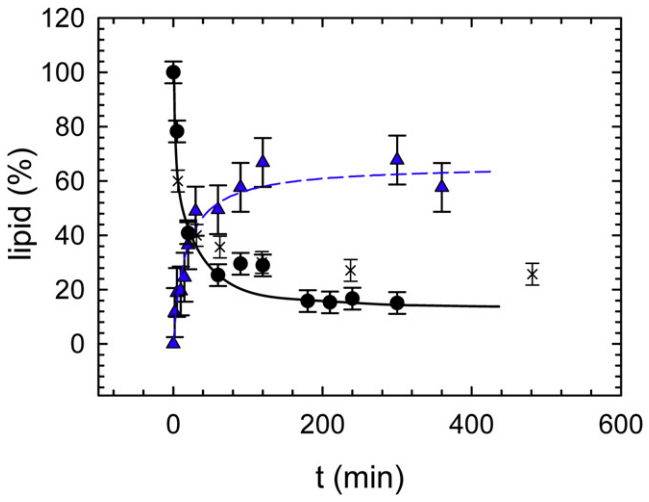

FIGURE 1 SM hydrolysis (*circles*) and generation of C16:0 Cer (*triangles*) by SMase in POPC/SM bilayers as determined by HPTLC. Crosses show apoptosis data on human leukemia cells from Tepper et al. (26). Lines show hyperbolic fits.

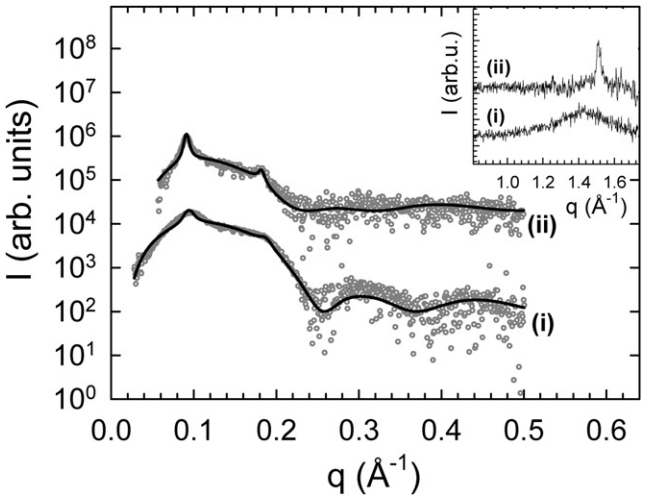

FIGURE 2 SAXS patterns of POPC/SM bilayers (*i*) before and (*ii*) 15.5 h after enzyme addition. Solid lines correspond to full q-range fits (21,22). Control experiments in the absence of SMase did not reveal any detectable changes to membrane structure. Corresponding WAXS data are shown in the inset. The patterns are vertically shifted for better graphical presentation.

Dynamic membrane structure effects

Structural changes occurring on the membrane level during the enzymatic hydrolysis of SM were followed by time-resolved SWAXS. Before the addition of SMase, SAXS data showed very broad first- and second-order Bragg reflections (Fig. 2). This indicates the presence of oligolamellar vesicles (OLVs) composed of about three positionally correlated bilayers with a lamellar repeat distance of $d = 64.6$ Å. This may come as a surprise, because the applied extrusion technique yielded LUVs with a narrow size distribution (Fig. S1 *A*). However, SAXS patterns are very sensitive to the presence of positionally correlated bilayers, which have a significantly stronger scattering signal than unilamellar vesicles (see Eq. 1). Thus, although LUVs are initially the major population of vesicles, OLVs are much more apparent. In support of this notion, a full q-range analysis of the diffraction pattern in terms of Eq. 1 gave $p_{diff} = 0.96 \pm 0.1$ as a lower limit for the fraction of LUVs. During the enzymatic reaction, the Bragg peaks sharpened considerably and their width finally corresponded to approximately seven positionally correlated bilayers and a repeat distance of $d =$ 68.7 Å. In addition, we analyzed an equivalent sample by photon correlation spectroscopy and found an additional population of vesicles ~700 nm in size (Fig. S1 *B*), indicating large aggregates, most likely MLVs, in agreement with the increase of positional correlations observed by SAXS.

From the full q-range analysis, we further found a cross-bilayer head-to-head distance of $d_{HH} = 40.8$ Å before addition of SMase, indicating a fluid phase, in agreement with WAXS data (see below) and previous reports (10). The final SAXS pattern corresponded to a d_{HH} of 45.2 Å, showing the formation of a gel phase. This is further substantiated by a comparison to membrane thickness data on POPC/SM/Cer mixtures under equilibrium conditions (10). There, too, it was found that Cer leads to macroscopic separation into fluid (L_α^c) and gel (L_β^c) phases.

Fig. 3, *A* and *B*, shows the corresponding time evolutions of the lamellar repeat distance, d, and the number of correlated bilayers, N_{layer}, respectively, during this transformation. We found a steep initial increase of d with a slope of 0.1 Å/min. After ~20 min, the slope of d decreased by roughly three orders of magnitude. At the same time, we observed a significantly slower increase of N_{layer}, which leveled off after ~170 min.

The changes in lateral packing of the membrane lipids associated with the changes in bilayer dimensions discussed

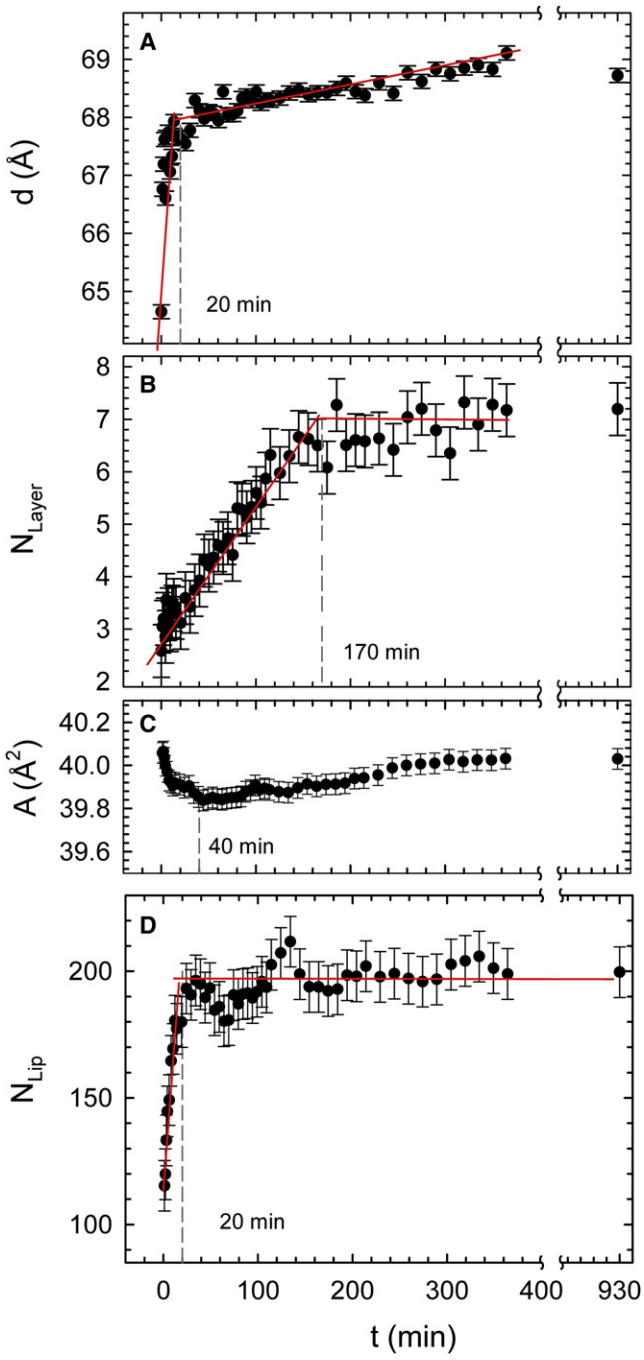

FIGURE 3 (*A*) Evolution of lamellar repeat distance, (*B*) average number of positionally correlated layers, (*C*) lateral area/lipid in the gel phase, and (*D*) average number of positionally correlated lipids/gel-phase domain during the enzyme reaction.

above are seen in the WAXS patterns (Fig. 2, *inset*). The advantage of these data in the case presented here is that WAXS originates from positional correlations of the hydrocarbon chains in the plane of the bilayer. Thus, the retrieved structural information is not affected by the presence of OLVs. Before enzyme addition, we observed a diffuse chain correlation peak centered at $q = 1.43$ Å^{-1}, typical for fluid hydrocarbon chains and, as expected from the temperature of our experiments, well above the melting transition of the POPC/SM equimolar mixture, $T_m \sim 25°C$ (29). The final WAXS pattern exhibited a peak at $q = 1.51$ Å^{-1}, demonstrating the generation of a L_β^c gel phase with a 2D hexagonal packing of the acyl chains and with a lateral area/lipid, A, of 40.0 Å^2, similar to reports from equilibrium studies with defined Cer concentrations (see, e.g., Pabst et al. (10)). From the peak width, we further estimate an average domain size of ~13 nm, corresponding to ~200 in-plane positionally correlated lipids.

The kinetics of the gel-phase domain formation is presented in Fig. 3, *C* and *D*. WAXS data showed the occurrence of a gel phase already at the onset of the experiment, i.e., 70 s after addition of SMase, where the lateral area/lipid, A, equaled the final value. However, the peak width indicated that N_{lip} was initially ~100 and reached its final value of ~200 after ~20 min. The growth rate was about four times faster than Cer generation (Fig. 1), but similar to the changes of d, as observed from SAXS. This demonstrates that the SAXS results are dominated by the generation of the L_β^c phase from LUVs and that the initial presence of a few OLVs is not relevant to the overall reaction kinetics. The lateral area/gel-phase lipid decreased at a rate similar to the rate of increase of N_{lip} and d. A showed a minimum value of 39.8 Å^2 after ~30–40 min and then increased slowly back to 40 Å^2. The increase of the WAXS peak intensities followed a double-exponential decay to maximum with a fast and a slow time constant of $t_1 \sim 6$ min and $t_2 \sim 116$ min, respectively (Fig. S2).

To gain deeper insight into the lamellar swelling that occurs during the reaction (Fig. 3 *A*), we studied MLVs of defined POPC/SM/Cer ratio under equilibrium conditions. Fig. 4 *A* shows the SAXS patterns of POPC/SM/Cer = 50/35/15 MLVs as a fully hydrated dispersion and under osmotic stress. Osmotic pressure was applied using PEG, as described in detail previously (10). Four lamellar diffraction orders were well-resolved for the fully hydrated sample. The fluid-gel phase coexistence described previously (see, e.g., (9,10)), with two lamellar lattices of $d = 64.2$ Å and $d = 54.0$ Å, became visible upon application of osmotic pressure ($\Pi = 4.2$ atm). The phase with the larger d-value corresponds to a L_β^c phase, rich in SM and Cer, whereas the small d-value reflects an L_α^c phase, rich in POPC (10). A full structural characterization of the model system presented here, to be published separately, demonstrates that the L_β^c phase coexists with an L_α^c phase at 37°C within the Cer concentration range used here.

Finally, we compared the d-values of the time-resolved study to equilibrium mixtures of various Cer concentrations (Fig. 4 *B*). In this experiment, SM was gradually replaced by C16:0 Cer to mimic SM hydrolysis, maintaining POPC/sphingolipid = 1. The d-spacings correspond to the weighted average of the lamellar repeat of fluid and the gel phases at each Cer concentration, because values for the coexisting

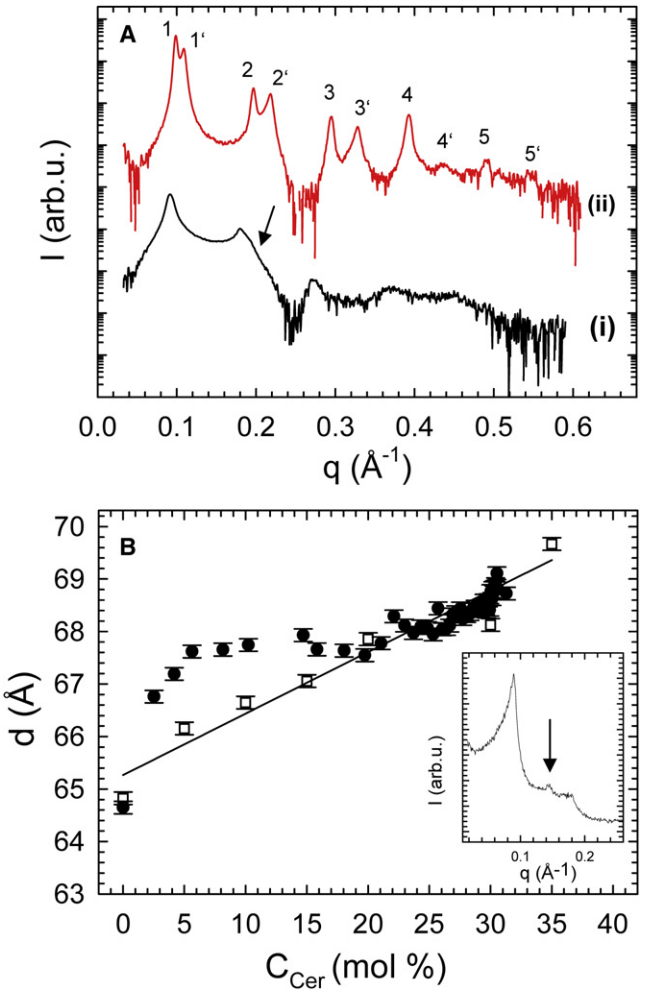

FIGURE 4 Comparison to equilibrium structural data. (*A*) SAXS patterns for POPC/SM/Cer = 50/35/15 without (*i*) and with (*ii*) osmotic pressure $\Pi = 4.2$ atm. The arrow indicates the asymmetry of the second-order peak due to the gel-fluid phase coexistence. Numbers 1, 2, 3, etc. refer to the lamellar diffraction orders of the gel and 1′, 2′, 3′, etc. to those of the fluid phases. (*B*) Comparison of *d*-values obtained during the enzyme reaction (*solid circles*) to equilibrium values (*open squares*) on a common C16:0 Cer concentration scale. (*Inset*) SAXS pattern at 35 mol % Cer exhibiting an additional peak (*arrow*) due to the presence of a pure Cer phase.

fluid and gel lattices partially overlap at full hydration (Fig. 4 *A*). The equilibrium *d*-values increased roughly linearly with Cer content, reflecting the increase of the $L_\beta{}^c$ phase fraction. At 35 mol % C16:0 Cer, we observed an additional Bragg peak with $d = 43.6$ Å, which corresponds to a pure Cer domain (30) (Fig. 4 *B*, *inset*). This shows that the solubility limit of Cer in this system is in the concentration range 30–35 mol %. A similar limit has been reported recently in SM/Cer monolayers (31), indicating that at high concentrations also, Cer interacts primarily with SM and not with POPC. For comparison with the values obtained during the enzyme reaction, the experimental time axis was converted into a Cer concentration axis by applying the fits to the C16:0 Cer generation data from HPTLC (Fig. 1). Note that the SM used here is mainly composed of C16:0 acyl chains. Hence, C16:0 Cer generation will dominate the evolution of *d* during SM hydrolysis. The results showed a significant deviation of *d*-values during the enzyme reaction from the linear increase under equilibrium conditions to ~20 mol % Cer, i.e., for the first ~20 min. At higher Cer concentrations, the enzymatic reaction essentially follows the equilibrium *d*-values. Together with the saturation behavior of SM degradation, this signifies also that the system is essentially in equilibrium 15.5 h after the addition of SMase.

DISCUSSION

On the basis of our results we are able to link the molecular events occurring in the course of SMase action to effects on the macroscopic level. The initiation of the enzyme reaction is the attachment of the enzyme to the vesicles, where it starts to hydrolyze the SM lipids of the outer membrane leaflet that leads to the formation of an L_β gel phase. As these domains grow in size, transbilayer coupling might occur at some point (32), leading to the formation of a gel phase in both monolayers, which may be further supported by Cer flip-flop (33). Asymmetric gelification of the outer membrane leaflet builds up a large mechanical strain due to differences in lateral area/lipid in the fluid and gel phase. At only 70 s after the start of the enzyme reaction, we found $A = 40$ Å^2 for the gel phase, which is ~20–25 Å^2 smaller than the area estimated for the POPC/SM mixture in the L_α phase (34,35). The spontaneous negative curvature of Cer given by its small headgroup size (36) imposes additional strain. This results in an invagination of the membrane, similar to bimetallic strips, budding, and finally shedding of vesicles in combination with transient pore formation (1,9,13,14).

We found an induction of the $L_\beta{}^c$ phase right at the onset of the enzyme reaction, and it is of interest that this domain size grows about four times faster than Cer is generated by SMase (Fig. 3 *C*). This can be understood by the ability of SM to form hydrogen bonds with Cer, which leads to a recruitment of SM to gel phase domains, as found in equilibrium studies (10,37). The rapid $L_\beta{}^c$ phase formation stops after ~20 min. The associated bilayer swelling, which proceeds initially at the same rate as gel-phase formation, also slowed down after ~20 min (Fig. 3 *A*). This corresponds to a reduction of SM to 46% (Fig. 1) and, hence, to a molar SM/Cer ratio of ~1. Thus, as long as Cer levels do not exceed those of SM, progression of the gel phase is faster than Cer generation. The growth of domain size stops for SM/Cer < 1. This can be rationalized by 1), the low affinity of POPC/Cer interactions (38), and 2), the entropic penalty of pairwise Cer interactions, which leads to segregation of membrane-insoluble Cer crystallites (Fig. 4 *B*, *inset*). Still, the amount of $L_\beta{}^c$ phase, but not its packing density, continues to grow, as shown by the continued increase of the average *d*-spacing (Fig. 3 *A*) and WAXS peak intensity. This growth is slow enough to follow equilibrium *d*-values (Fig. 4 *B*). However, because Cer levels

are larger than those of SM (SM/Cer < 1), POPC is increasingly incorporated into the gel domains, in agreement with previous reports that show the induction of a gel phase in POPC bilayers by Cer (39,40). This scenario is substantiated by the recovery of the lateral area/lipid after 40 min (Fig. 3 *C*), which is related to the larger lateral size of POPC compared to SM due to its monounsaturated acyl chain.

In agreement with previous biophysical studies (13,14), we also found an aggregation of membranes (Fig. 3 *B*). However, growth of regularly stacked bilayers proceeded significantly more slowly than did gel phase formation and bilayer swelling. This is expected, because the removal of interstitial water and membrane diffusion processes proceed on a slower timescale than gel phase formation. Since the SAXS signal is dominated by the $L_\beta{}^c$ phase, the physical origin of vesicle aggregation during the action of SMase can be understood as follows. The gel phase macroscopically separates from the coexisting $L_\alpha{}^c$ phase. Gel-phase bilayers are rigid and exhibit negligible bending undulations, which are the source of a long-range repulsive force in fluid (soft) membranes (see, e.g., Pabst et al. (10)). In the absence of this force, adhesion between gel-phase membranes increases. In addition, the thicker gel membranes also experience increased van der Waals attraction. In turn, attractive interactions between macroscopically phase-separated $L_\alpha{}^c$ domains are much weaker. Hence, they may remain positionally uncorrelated, accounting for the absence of their signature in the SAXS data (Fig. 2). Comparing these results to those from previous studies on SMase activity (13,14,41), we generally find differences in timescales on the order of one magnitude. For example, aggregation of vesicles (13,14) was found to proceed on the timescale of seconds, whereas we observe a growth rate of stacked bilayers of several minutes. Most likely, this is related to differences in enzyme/SM ratios and/or composition of lipid model membranes as the physical state of membranes was demonstrated to influence SM hydrolysis (42,43).

Finally, we focus on the saturation level of Cer, which is at ~86% and indicates that SM is not fully hydrolyzed, although SMase has full access to all SM upon entry into the vesicles. One of the more obvious reasons could be that the enzyme gets entrapped during the various vesiculation processes, making a fraction of SM inaccessible to SMase. Another possibility is that the affinity of the SMase to the lipid surface decreases with an increase of POPC relative to SM (44). However, it is also remarkable that we did not observe any pure Cer aggregates. C16:0 Cer aggregates are readily detectable by SAXS in equilibrium systems (Fig. 4 *B*). Clearly, we cannot assume that the system is fully equilibrated 15.5 h after the start of the enzyme reaction. However, even if the reaction were to proceed with similar kinetics for two more months, the additional increase of Cer would be only 1%. At the same time, it is also important to realize that our conclusions do not really depend on equilibrium. Apoptotic cells are disposed by macrophages long before thermal equilibrium has been reached. Agreement of our data on SM degradation with those of cell biological experiments (Fig. 1) demonstrates similar timescales. On this timescale, Cer remains dissolved within the membrane. Hence, catalytic turnover stops just at the solubility limit of Cer in POPC/SM membranes. We therefore speculate that there is a mechanical feedback mechanism, realized, for example, by changes of lateral pressure at the lipid/water interface, which stops SMase activity, similar to a recent suggestion for the regulation of lipid biosynthesis in *Acholeplasma laidlawii* (45). Indeed, it has been reported that SMase activity depends on the fluidity of model membranes (42,43), and we have demonstrated previously that Cer affects the bending rigidity of both coexisting phases (10). It is interesting that in different cell biology experiments (26–28), SM hydrolysis stopped at about the same Cer concentration. This suggests that a similar feedback system may be also present in cells, which could be a natural control mechanism to reduce toxic risks of pure Cer aggregates (46).

The agreement with in vitro studies is even more surprising, considering that our model system did not contain cholesterol, which is a major component of mammalian plasma membranes. It has been suggested that cholesterol competes with ceramide and may dissolve Cer-enriched gel domains at high concentrations, although it is displaced from raftlike domains at low concentrations (47,48). Moreover, cholesterol was shown to increase SMase activity at high concentrations in binary mixtures with SM (49). However, it has been shown also that morphological changes induced by SMase differ significantly in lipid mixtures with an additional unsaturated lipid component (15,50). The essential difference between POPC/SM bilayers and POPC/SM/cholesterol membranes is a macroscopic fluid-fluid phase separation occurring in the latter system before the addition of SMase (15). Nevertheless, if SMase activity depends strictly on the SM/Cer molar ratio, such preexisting lateral structures might even be irrelevant to the overall enzyme kinetics. At least, this would explain the agreement to cell biological data. Future studies planned in our laboratory will address this issue.

CONCLUSIONS

In summary, we found that the SM/Cer molar ratio strongly affects membrane structural rearrangement through formation of gel-phase domains during the action of SMase (Fig. 5). As long as each Cer has at least one SM partner, $L_\beta{}^c$ phase formation proceeds faster than enzymatic Cer generation. Gel-phase domains lead to membrane aggregation because of increased adhesive forces. If Cer levels exceed those of SM, POPC is increasingly incorporated into the gel phase until the reaction stops just below the solubility limit of Cer in membranes. Similar kinetics and SM saturation levels in cell biology studies suggest that the evolution of apoptosis is influenced to a large extent by

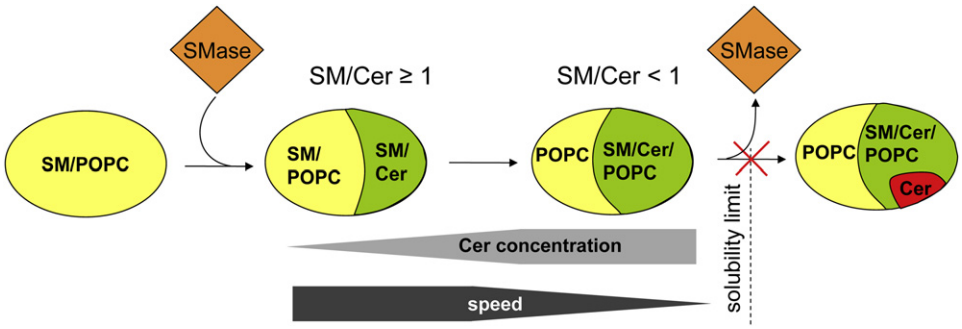

FIGURE 5 Schematic of SMase activity as a function of the SM/Cer molar ratio. Addition of SMase to SM/POPC vesicles induces a macroscopic phase separation into SM/Cer-rich gel and SM/POPC-rich fluid domains. As long as SM/Cer $\geq$ 1, each Cer can pair with at least one SM and the progress of gel-phase formation is faster than Cer generation. For SM/Cer $<$ 1, kinetics slow down, because POPC, which has a lower affinity to Cer, needs to be incorporated into the growing gel domains to avoid precipitation of Cer crystallites. The reaction stops just at the solubility limit of Cer within the membrane.

membrane lipids and their mechanical coupling to SMase activity.

SUPPORTING MATERIAL

Two figures are available at http://www.biophysj.org/biophysj/supplemental/S0006-3495(10)0526-6.

We are grateful to Edgar Gander, Ruth Prassl, and Michael Rappolt for valuable help in this study. We further thank Albin Hermetter for critical reading of the manuscript.

REFERENCES

1. Kolesnick, R. N., F. M. Goñi, and A. Alonso. 2000. Compartmentalization of ceramide signaling: physical foundations and biological effects. *J. Cell. Physiol.* 184:285–300.
2. van Blitterswijk, W. J., A. H. van der Luit, …, J. Borst. 2003. Ceramide: second messenger or modulator of membrane structure and dynamics? *Biochem. J.* 369:199–211.
3. Hannun, Y. A., and L. M. Obeid. 2008. Principles of bioactive lipid signalling: lessons from sphingolipids. *Natl. Rev.* 9:139–150.
4. Fruhwirth, G. O., and A. Hermetter. 2008. Mediation of apoptosis by oxidized phospholipids. *Subcell. Biochem.* 49:351–367.
5. Pike, L. J. 2006. Rafts defined: a report on the Keystone symposium on lipid rafts and cell function. *J. Lipid Res.* 47:1597–1598.
6. Lingwood, D., and K. Simons. 2010. Lipid rafts as a membrane-organizing principle. *Science.* 327:46–50.
7. Elmore, S. 2007. Apoptosis: a review of programmed cell death. *Toxicol. Pathol.* 35:495–516.
8. Gulbins, E., S. Dreschers, …, H. Grassmé. 2004. Ceramide, membrane rafts and infections. *J. Mol. Med.* 82:357–363.
9. Goñi, F. M., and A. Alonso. 2009. Effects of ceramide and other simple sphingolipids on membrane lateral structure. *Biochim. Biophys. Acta.* 1788:169–177.
10. Pabst, G., B. Boulgaropoulos, …, P. Laggner. 2009. Effect of ceramide on nonraft proteins. *J. Membr. Biol.* 231:125–132.
11. Andrieu-Abadie, N., and T. Levade. 2002. Sphingomyelin hydrolysis during apoptosis. *Biochim. Biophys. Acta.* 1585:126–134.
12. Rudolf, E., and M. Cervinka. 2005. Membrane blebbing in cancer cells treated with various apoptotic inducers. *Acta Medica (Cordoba).* 48:29–34.
13. Ruiz-Argüello, M. B., G. Basáñez, …, A. Alonso. 1996. Different effects of enzyme-generated ceramides and diacylglycerols in phospholipid membrane fusion and leakage. *J. Biol. Chem.* 271:26616–26621.
14. Holopainen, J. M., M. I. Angelova, and P. K. Kinnunen. 2000. Vectorial budding of vesicles by asymmetrical enzymatic formation of ceramide in giant liposomes. *Biophys. J.* 78:830–838.
15. Chao, L., A. P. Gast, …, K. F. Jensen. 2010. Sphingomyelinase-induced phase transformations: causing morphology switches and multiple-time-domain ceramide generation in model raft membranes. *Langmuir.* 26:344–356.
16. Ayuyan, A. G., and F. S. Cohen. 2006. Lipid peroxides promote large rafts: effects of excitation of probes in fluorescence microscopy and electrochemical reactions during vesicle formation. *Biophys. J.* 91:2172–2183.
17. Zhao, J., J. Wu, …, G. Feigenson. 2007. Phase studies of model biomembranes: macroscopic coexistence of $L_\alpha + L_\beta$, with light-induced coexistence of $L_\alpha + L_o$ phases. *Biochim. Biophys. Acta.* 1768: 2777–2786.
18. Veatch, S. L., S. S. Leung, …, J. L. Thewalt. 2007. Fluorescent probes alter miscibility phase boundaries in ternary vesicles. *J. Phys. Chem. B.* 111:502–504.
19. Ago, H., M. Oda, …, J. Sakurai. 2006. Structural basis of the sphingomyelin phosphodiesterase activity in neutral sphingomyelinase from *Bacillus cereus*. *J. Biol. Chem.* 281:16157–16167.
20. Contreras, F. X., A. V. Villar, …, F. M. Goñi. 2003. Sphingomyelinase activity causes transbilayer lipid translocation in model and cell membranes. *J. Biol. Chem.* 278:37169–37174.
21. Pabst, G., M. Rappolt, …, P. Laggner. 2000. Structural information from multilamellar liposomes at full hydration: full *q*-range fitting with high quality x-ray data. *Phys. Rev. E Stat. Phys. Plasmas Fluids Relat. Interdiscip. Topics.* 62(3 Pt B):4000–4009.
22. Pabst, G., R. Koschuch, …, P. Laggner. 2003. Structural analysis of weakly ordered membrane stacks. *J. Appl. Cryst.* 63:1378–1388.
23. Pabst, G., S. Danner, …, V. A. Raghunathan. 2007. On the propensity of phosphatidylglycerols to form interdigitated phases. *Biophys. J.* 93: 513–525.
24. Warren, B. E. 1941. X-ray diffraction methods. *J. Appl. Phys.* 12: 375–383.
25. McIntosh, T. J., and S. A. Simon. 1986. Area per molecule and distribution of water in fully hydrated dilauroylphosphatidylethanolamine bilayers. *Biochemistry.* 25:4948–4952.
26. Tepper, A. D., P. Ruurs, …, W. J. van Blitterswijk. 2000. Sphingomyelin hydrolysis to ceramide during the execution phase of apoptosis results from phospholipid scrambling and alters cell-surface morphology. *J. Cell Biol.* 150:155–164.
27. Ohvo, H., C. Olsio, and J. P. Slotte. 1997. Effects of sphingomyelin and phosphatidylcholine degradation on cyclodextrin-mediated cholesterol efflux in cultured fibroblasts. *Biochim. Biophys. Acta.* 1349:131–141.
28. Andrieu, N., R. Salvayre, and T. Levade. 1996. Comparative study of the metabolic pools of sphingomyelin and phosphatidylcholine sensitive to tumor necrosis factor. *Eur. J. Biochem.* 236:738–745.

29. Degovics, G., A. Latal, …, K. Lohner. 1997. Structure and thermotropic behaviour of mixed choline phospholipid model membranes. *J. Appl. Cryst.* 30:776–780.

30. Shah, J., J. M. Atienza, …, G. G. Shipley. 1995. Physical properties of ceramides: effect of fatty acid hydroxylation. *J. Lipid Res.* 36: 1945–1955.

31. Busto, J. V., M. L. Fanani, …, A. Alonso. 2009. Coexistence of immiscible mixtures of palmitoylsphingomyelin and palmitoylceramide in monolayers and bilayers. *Biophys. J.* 97:2717–2726.

32. May, S. 2009. Trans-monolayer coupling of fluid domains in lipid bilayers. *Soft Matter.* 5:3148–3156.

33. Contreras, F. X., G. Basañez, …, F. M. Goñi. 2005. Asymmetric addition of ceramides but not dihydroceramides promotes transbilayer (flip-flop) lipid motion in membranes. *Biophys. J.* 88:348–359.

34. Chiu, S. W., S. Vasudevan, …, H. L. Scott. 2003. Structure of sphingomyelin bilayers: a simulation study. *Biophys. J.* 85:3624–3635.

35. Pabst, G., A. Hodzic, …, P. Laggner. 2007. Rigidification of neutral lipid bilayers in the presence of salts. *Biophys. J.* 93:2688–2696.

36. Veiga, M. P., J. L. Arrondo, …, A. Alonso. 1999. Ceramides in phospholipid membranes: effects on bilayer stability and transition to nonlamellar phases. *Biophys. J.* 76:342–350.

37. Castro, B. M., R. F. de Almeida, …, M. Prieto. 2007. Formation of ceramide/sphingomyelin gel domains in the presence of an unsaturated phospholipid: a quantitative multiprobe approach. *Biophys. J.* 93: 1639–1650.

38. Silva, L. C., R. F. de Almeida, …, M. Prieto. 2007. Ceramide-domain formation and collapse in lipid rafts: membrane reorganization by an apoptotic lipid. *Biophys. J.* 92:502–516.

39. Silva, L., R. F. M. de Almeida, …, M. Prieto. 2006. Ceramide-platform formation and -induced biophysical changes in a fluid phospholipid membrane. *Mol. Membr. Biol.* 23:137–148.

40. Fidorra, M., L. Duelund, …, L. A. Bagatolli. 2006. Absence of fluid-ordered/fluid-disordered phase coexistence in ceramide/POPC mixtures containing cholesterol. *Biophys. J.* 90:4437–4451.

41. Holopainen, J. M., M. Subramanian, and P. K. Kinnunen. 1998. Sphingomyelinase induces lipid microdomain formation in a fluid phosphatidylcholine/sphingomyelin membrane. *Biochemistry.* 37: 17562–17570.

42. Ruiz-Argüello, M. B., M. P. Veiga, …, A. Alonso. 2002. Sphingomyelinase cleavage of sphingomyelin in pure and mixed lipid membranes. Influence of the physical state of the sphingolipid. *Chem. Phys. Lipids.* 114:11–20.

43. Goñi, F. M., and A. Alonso. 2002. Sphingomyelinases: enzymology and membrane activity. *FEBS Lett.* 531:38–46.

44. Yu, B. Z., D. Zakim, and M. K. Jain. 2002. Processive interfacial catalytic turnover by *Bacillus cereus* sphingomyelinase on sphingomyelin vesicles. *Biochim. Biophys. Acta.* 1583:122–132.

45. Alley, S. H., O. Ces, …, M. Barahona. 2008. Biophysical regulation of lipid biosynthesis in the plasma membrane. *Biophys. J.* 94:2938–2954.

46. Shabbits, J. A., and L. D. Mayer. 2003. Intracellular delivery of ceramide lipids via liposomes enhances apoptosis in vitro. *Biochim. Biophys. Acta.* 1612:98–106.

47. Sot, J., M. Ibarguren, …, A. Alonso. 2008. Cholesterol displacement by ceramide in sphingomyelin-containing liquid-ordered domains, and generation of gel regions in giant lipidic vesicles. *FEBS Lett.* 582: 3230–3236.

48. Castro, B. M., L. C. Silva, …, M. Prieto. 2009. Cholesterol-rich fluid membranes solubilize ceramide domains: implications for the structure and dynamics of mammalian intracellular and plasma membranes. *J. Biol. Chem.* 284:22978–22987.

49. Contreras, F. X., J. Sot, …, F. M. Goñi. 2004. Cholesterol modulation of sphingomyelinase activity at physiological temperatures. *Chem. Phys. Lipids.* 130:127–134.

50. Fanani, M. L., L. De Tullio, …, B. Maggio. 2009. Sphingomyelinase-induced domain shape relaxation driven by out-of-equilibrium changes of composition. *Biophys. J.* 96:67–76.